Fission and deep-inelastic scattering yields for $^{58}Ni + ^{112,124}Sn$ at energies around the barrier

F. L. H. Wolfs
Argonne National Laboratory, Argonne, Illinois 60439
and University of Chicago, Chicago, Illinois 60637
(Received 1 June 1987)

Excitation functions of deep-inelastic scattering and fission have been measured for $^{58}Ni + ^{112,124}Sn$ at bombarding energies between 230 and 290 MeV. It is found that even at energies below the Coulomb barrier deep-inelastic scattering is an important reaction channel with yields similar to that of fusion. The total reaction cross sections are now in good agreement with the sum of the measured fusion, deep-inelastic, and quasielastic scattering yields. Attempts to reproduce the sub-barrier fusion yields by coupled-channels calculations are discussed.

I. INTRODUCTION

Although in recent years considerable attention has been paid to the study of heavy-ion reactions at energies in the vicinity of the Coulomb barrier, only limited information exists on the strength of reaction processes other than fusion. In order to study the distribution of the total reaction strength among the various reaction modes, the evaporation residue, fission, and quasielastic scattering yields were measured previously for $^{58}Ni + ^{112-124}Sn$ at energies around the Coulomb barrier.[1-4] The total reaction cross sections, deduced from the measured elastic plus inelastic scattering angular distributions, were not accounted for by the sum of the observed yields (see Fig. 1). The reaction mode that is most likely to have been missed in the previous measurements is one that may be related to deep-inelastic scattering, a process where all the incident kinetic energy is rapidly dissipated and the two fragments (with masses near those of the projectile and target) emerge with energies well below the Coulomb repulsion energy of two touching spherical nuclei, possibly from a strongly deformed system.

In this paper results are presented of the measurement of the fission and deep-inelastic scattering cross sections for $^{58}Ni + ^{112,124}Sn$ at laboratory energies between 230 and 290 MeV, corresponding to energies from 20 MeV below to 50 MeV above the Coulomb barrier [calculated with $R_b = 1.4(A_p^{1/3} + A_t^{1/3})$ fm]. A first report of these results for $^{58}Ni + ^{124}Sn$ has been submitted for publication.[5] In Sec. II the experimental technique will be presented, together with some aspects of the data analysis. In Sec. III the experimental results are discussed and compared with results from a previous experiment.[2,3] In Sec. IV the deep-inelastic scattering cross sections are compared with results from friction model calculations, the decomposition of the total reaction cross section is discussed, and the sub-barrier fusion yields are compared with model calculations.

II. EXPERIMENTAL METHOD

^{58}Ni beams from the Argonne Tandem-Linac Accelerator System (ATLAS) were incident on isotopically enriched $^{112,124}Sn$ targets (80 $\mu g/cm^2$ ^{112}Sn, 99.9% enriched, and 50 $\mu g/cm^2$ ^{124}Sn, 96% enriched, both on 10–20 $\mu g/cm^2$ carbon), mounted in the center of a 165 cm diameter scattering chamber. The beam spot on the target was defined by a set of circular collimators to less than 3 mm. Beam currents measured in the Faraday cup behind the target were typically 1–2 particle nA.

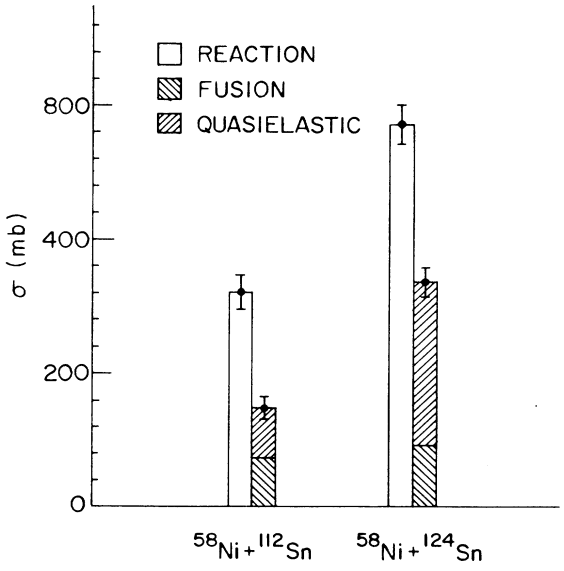

FIG. 1. Comparison of the total reaction cross sections deduced from the previously measured elastic plus inelastic scattering angular distributions (Ref. 4) and the sum of previously measured fusion (Ref. 3) and quasielastic scattering (Ref. 4) yields for $^{58}Ni + ^{112}Sn$ and $^{58}Ni + ^{124}Sn$ at laboratory energies of 253.7 and 245.8 MeV, respectively.

The stability of the beam and the target quality were monitored with three silicon surface barrier detectors.

Reaction products were detected in coincidence with two large-area (20×20 cm^2), position-sensitive, parallel-grid avalanche counters (PGAC's), 40 cm from the target. The principle of operation of the PGAC's, which were especially developed for this measurement, is very similar to that of a parallel plate avalanche counter (PPAC),[6–9] the difference being that the foils customarily used for anodes and cathodes in a PPAC have been replaced by wire grids. A PGAC was preferred over a PPAC due to its lower detection energy threshold ($\simeq 10$ MeV for ^{124}Sn ions). The counters provided a fast timing signal (extracted from the anode) and position signals (extracted from the position wire planes using delay-line readout). The timing signal from each detector was used to determine whether there was a coincidence, which was defined as an event in both detectors within 200 ns, and to start a time-to-digital converter (TDC) for the position measurements. The TDC's were stopped with the signals from both ends of the delay lines of the corresponding detector. The absolute time of flight of the two reaction products with respect to the rf time structure of the accelerator, and their time-of-flight difference were also measured. The data were monitored on line and written event by event onto magnetic tape. The detector signals were calibrated using the elastic scattering of ^{58}Ni ions from a thin ^{197}Au target and a mask with 40 collimator holes. The intrinsic position and timing resolution of each detector were 0.5 mm and 275 ps, respectively.

From the scattering angles of the two reaction products and their relative time of flight, their masses and energies can be calculated, assuming a two-body final state. The mass resolution obtained was 2.5 u [full width at half maximum (FWHM)], a large fraction of it due to energy and angle straggling in the target. The energy resolution was ~ 10 MeV. During the analysis, events were only accepted if the two reaction products were in the reaction plane within $\pm 2.5°$. This limit will include those events in which the direction of the reaction products may be slightly changed due to the evaporation of light particles. Events from scattering by target contaminants were rejected using the measured absolute time of flight of both reaction products to calculate the sum of the fragment masses, which does not require a knowledge of the actual target mass.

The monitor yields were used for relative normalization between different runs. Absolute cross sections were obtained by normalizing the number of elastic events at the most forward angles to the corresponding Rutherford cross sections. The accuracy of this procedure is estimated to be about 10%. The data were corrected event by event for the geometrical detector efficiency which is a function of the detector position and the reaction kinematics.

III. EXPERIMENTAL RESULTS

Figure 2 shows mass spectra obtained for ^{58}Ni + ^{124}Sn at $E_{\rm lab}=290$ MeV, gated on various Q values. The mass distributions for events with a Q value more negative than -20 MeV show two distinct components: two peaks centered around a mass close to that of the projectile and target (width ~ 10 u) and a wide mass distribution centered around half that of the compound nucleus

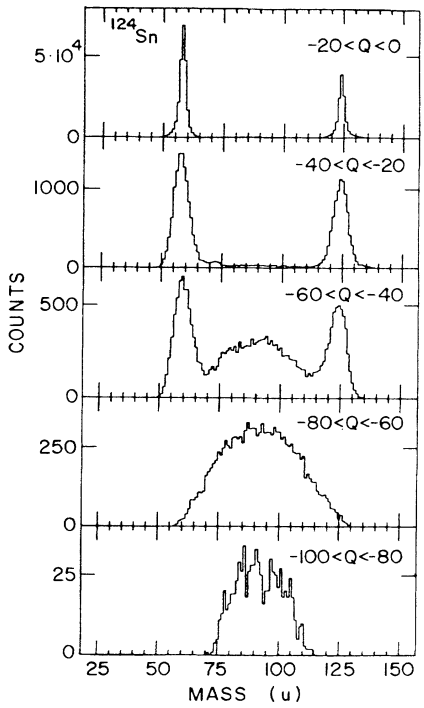

FIG. 2. Mass spectra for ^{58}Ni + ^{124}Sn at 290 MeV, gated on different Q values (shown in MeV).

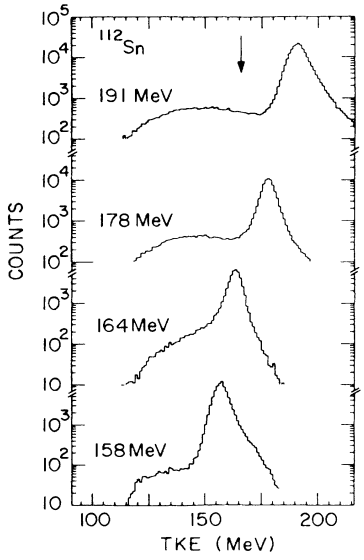

FIG. 3. Total kinetic energy (TKE) spectra of events with mass between 48 and 68 u, for ^{58}Ni + ^{112}Sn at various incident center-of-mass energies. The arrow indicates the TKE corresponding to the Coulomb repulsion energy of two touching spherical nuclei.

(width 30–40 u), consistent with fission. Figures 3 and 4 show total kinetic energy (TKE) spectra for events with masses between 48 and 68 u for ^{58}Ni + ^{112,124}Sn at various bombarding energies, obtained with the two detectors at 37.5° and 52.5°. This detector geometry allows the detection of events with Q values as negative as −120 MeV, and the observed low energy cutoff in the TKE spectra is therefore not related to a change in the coincident detection efficiency. The arrows in Figs. 3 and 4 indicate the TKE corresponding to the Coulomb repulsion energy of two touching spherical nuclei. The asymmetry of the peaks associated with quasielastic scattering towards higher energies is due to the deterioration of the Sn targets during the experiment as can be shown using detector simulations.

Based on the results shown in Figs. 2–4, I have defined deep-inelastic scattering events as those with mass close to the mass of projectile and target ($|\Delta m| < 10$ u) and with a reaction Q value more negative than −20 MeV. The TKE spectra show a distinct plateau for more negative Q values. As has been observed for many other systems[10–14] at energies above the Coulomb barrier, the low energy cutoff in the total kinetic energy of the deep-inelastic fragments is rather independent of bombarding energy and much smaller than the Coulomb repulsion energy of two touching spherical nuclei. Figures 3 and 4 show that the lower endpoints of the TKE spectra are located at around 120 MeV for both ^{112}Sn and ^{124}Sn, independent of incident energy, and consistent with a deformation in each reaction product of $\beta \simeq 0.65$.

Figures 5 and 6 show as examples angular distributions for deep-inelastic scattering for ^{58}Ni + ^{112,124}Sn for events with Q value between −60 and −40 MeV. The total angle- and energy-integrated deep-inelastic scattering yields of course include contributions from all events with Q value more negative than −20 MeV. The angular distributions in Figs. 5 and 6 reveal two components; one is peaked around an angle close to the grazing angle; the other shows an increase towards forward scattering angles. The deep-inelastic scattering yields were extracted from the measured angular distributions by fitting the yields in the vicinity of the grazing angle with a Gaussian and arbitrarily assuming a linear dependence of the yields as function of angle in the forward region. This assumption has little effect on the measured total deep-inelastic scattering cross sections, since at all but the lowest bombarding energy the component peaking near the grazing angle dominates. The errors in the yields of the forward peaked component of the angular distributions were estimated by using different functions to extrapolate to forward angles, including an exponential increase towards 0° and a constant $d\sigma/d\Omega$ between the most forward observed angle and 0°. The dashed curves in Fig. 6 show some of the fits used to obtain estimates of uncertainties.

Fission was defined as events with fragment masses be-

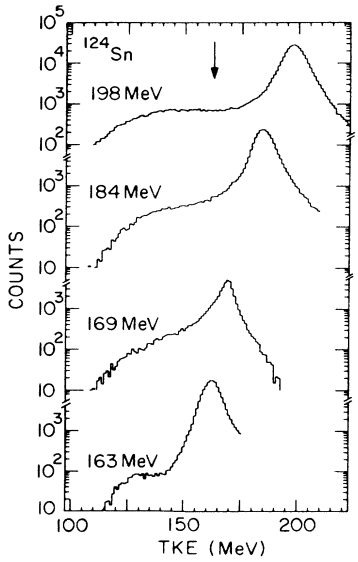

FIG. 4. Total kinetic energy (TKE) spectra of events with mass between 48 and 68 u, for ^{58}Ni + ^{124}Sn at various incident center-of-mass energies. The arrow indicates the TKE corresponding to the Coulomb repulsion energy of two touching spherical nuclei.

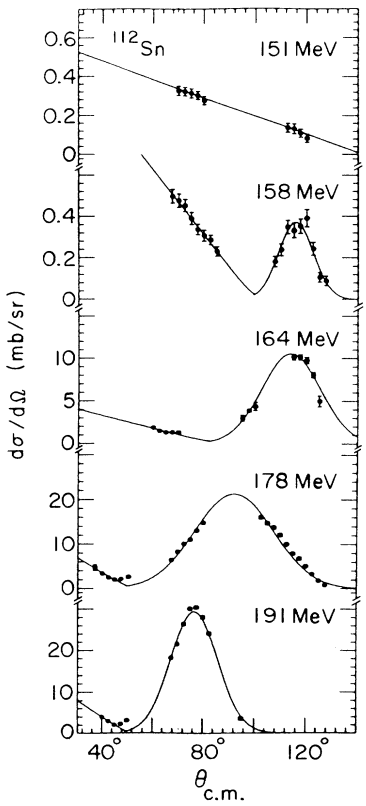

FIG. 5. Measured deep-inelastic scattering angular distributions for ^{58}Ni + ^{112}Sn for events with Q value between −40 and −60 MeV at various incident center-of-mass energies. Curves shown are fits to the data used to extract the total deep-inelastic scattering yields.

tween that of the projectile and target and a net mass transfer of at least 10 u (see Fig. 2). The fission yields were obtained from the measured angular distributions assuming a $1/\sin(\theta)$ dependence to extrapolate to the very forward and backward angles. This assumption is only valid in the limit of rapidly rotating systems; at energies around the Coulomb barrier the difference between the total fission cross sections obtained from fitting the measured angular distributions using the statistical model of fission and those obtained assuming a $1/\sin(\theta)$ dependence can be at most 25%.[3] However, my fission data do not cover the very forward and backward angles where fission angular distributions of the statistical model start deviating from a $1/\sin(\theta)$ dependence and therefore no attempt has been made to obtain total fission yields using statistical model fits.

Fission yields for ^{58,64}Ni + $^{112-124}$Sn have been measured previously by Lesko *et al.*[2,3] using the kinematic coincidence technique with a silicon surface barrier detector telescope and a position sensitive ionization counter. Their data for ^{58}Ni + ^{112,124}Sn are compared with my data in Fig. 7. For ^{58}Ni + ^{112}Sn both data sets are in good agreement. For ^{58}Ni + ^{124}Sn the fission cross sections reported here agree at the lowest and highest energies with their results, but are larger at intermediate energies. Since the present experiment allowed a cleaner separation between fission and quasielastic and deep-inelastic scattering I have only used the current results.

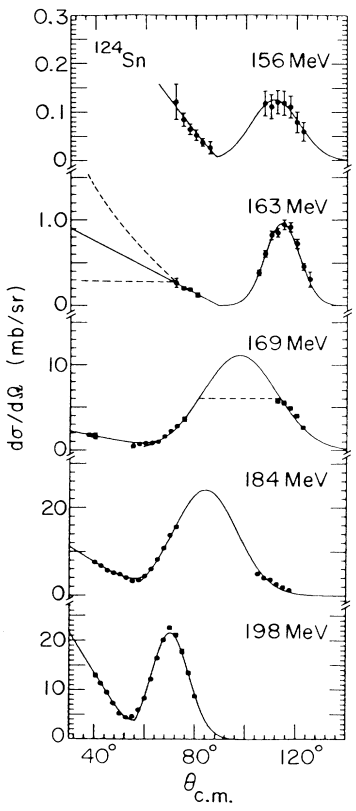

FIG. 6. Measured deep-inelastic scattering angular distributions for ^{58}Ni + ^{124}Sn for events with Q value between -40 and -60 MeV at various incident center-of-mass energies. Curves shown are fits to the data used to extract the total deep-inelastic scattering yields. The dashed curves show some of the fits used to obtain error estimates.

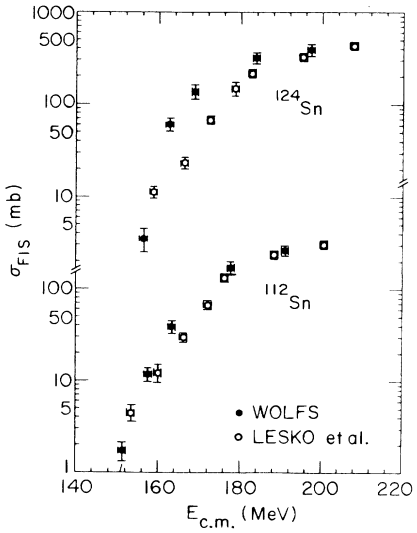

FIG. 7. Measured fission yields for ^{58}Ni + ^{112,124}Sn compared with those previously measured by Lesko *et al.* (Refs. 2 and 3).

The average fission Q value is independent of the scattering angle and more negative than the Coulomb repulsion energy of two touching spherical nuclei. At 290 MeV the measured average fission Q values are in good agreement with the Viola systematics.[15] At the lower bombarding energies the average kinetic energy of the fission fragments decreases with decreasing excitation energy of the compound nucleus, which can be understood in terms of a change the average spin of the compound nucleus.

IV. DISCUSSION

A. Deep-inelastic scattering

The mass spectra of deep-inelastic scattering events for ^{58}Ni + ^{112,124}Sn are peaked around masses close to those of the projectile and target. This has been observed for other systems at energies above the Coulomb barrier and is consistent with the picture that at energies around and below the barrier deep-inelastic scattering is governed by the equilibration of the charge asymmetry degree of freedom, and the interaction time is not long enough for the equilibration of the mass asymmetry degree of freedom to become important.[16]

Dissipative phenomena in heavy-ion reactions at energies above the Coulomb barrier can be treated in a classical approximation by introducing a frictional force which governs the transfer of kinetic energy to internal degrees of freedom of the reaction products. I have compared my deep-inelastic scattering data with predic-

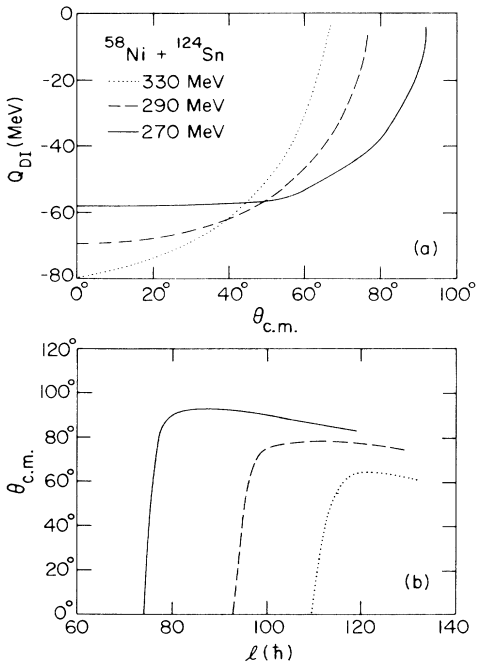

FIG. 8. Results of calculations using the one-body dissipation model for ^{58}Ni + ^{124}Sn at 270, 290, and 330 MeV.

tions of the one-body dissipation code developed by Feldmeier.[17] Due to its assumptions this model only works at incident energies above the Coulomb barrier and I can only compare the calculations with my data at 270 and 290 MeV. Some results of the calculations for ^{58}Ni + ^{124}Sn at $E_{lab}=270$, 290, and 330 MeV are shown in Fig. 8. The angular distributions are related to the calculated deflection functions by

$$\frac{d\sigma}{d\Omega}=\frac{\hbar^2}{2\mu E_{c.m.}}\left[\sin(\theta)\frac{1}{L}\frac{d\theta}{dL}\right]^{-1},$$

where μ is the reduced mass of the system. They have an orbiting component extending towards forward angles as well as a component that peaks near grazing angle, in qualitative agreement with my measured deep-inelastic scattering angular distributions. The cross sections for these two components at $E_{lab}=270$ and 290 MeV, obtained from these angular distributions, are listed in Table I and are compared with the measured yields. The calculated and measured yields for the orbiting component are in reasonable agreement but the calculated strength of the component peaked near the grazing angle is significantly smaller than the measured cross sections.

B. Decomposition of the total reaction cross section

The total reaction cross sections may, in principle, be deduced from the quarter-point for elastic scattering in an almost model-independent way.[18] However, in this measurement elastic scattering could not be separated from quasielastic scattering and the quarter-point recipe could not be used. Therefore, the total reaction cross sections were obtained from coupled-channels calculations with the code PTOLEMY[19] including inelastic excitation of the lowest 2^+ and 3^- states in projectile and target. The potential parameters were chosen such that the sum of the calculated elastic and inelastic scattering angular distributions reproduced the previously measured "elastic plus inelastic" scattering angular distributions at 245.8 and 253.7 MeV (Ref. 4) and at 330 MeV.[20] The optical model parameters used were $V=100$ MeV, $r_0=1.14$ fm, $a=0.71$ fm (0.75 fm for ^{124}Sn), $W=24$ MeV, $r_{i0}=1.26$ fm, and $a_i=0.54$ fm (0.60 fm for ^{124}Sn). Since experimentally it is difficult to separate elastic scattering from inelastic excitation of the low lying states in projectile and target, neither the measured nor the calculated total reaction cross sections will include the inelastic scattering yields. The calculated total reaction cross sections are listed in Table II. The errors reflect the uncertainty in the optical model parameters.

The quasielastic scattering yields were obtained by linear interpolation between the low energy measurements of Betts *et al.*[21] and the measured yields at two energies above the Coulomb barrier[4,20] and are listed in Table II. In Ref. 20 the separation between deep-inelastic and quasielastic scattering was based on the measured angular distributions and therefore the quasielastic scattering yields in Ref. 20 will also contain contributions from events with a Q value more negative than -20 MeV. However, if a cut at -20 MeV would have been used, the quasielastic yields in Ref. 20 would not change by more than 20% and the resulting changes in the interpolated quasielastic scattering cross sections used in this paper are within the errors. In principle, nuclear inelastic excitation is a quasielastic reaction channel. However, since the coupled-channels calcula-

TABLE I. Comparison between the measured and calculated deep-inelastic scattering yields for ^{58}Ni + ^{112,124}Sn at 270 and 290 MeV. The calculations are described in the text.

		Calculation		Experiment	
Target	$E_{c.m.}$ (MeV)	σ_{peak} (mb)	$\sigma_{forward}$ (mb)	σ_{peak} (mb)	$\sigma_{forward}$ (mb)
^{112}Sn	191.1	57	93	100±15	65±30
	177.9	44	36	135±20	30±15
^{124}Sn	197.6	118	124	130±20	100±50
	184.0	58	44	170±25	55±30

TABLE II. Comparison of the sum of the measured cross sections for evaporation residues, fusion, deep-inelastic, and quasielastic scattering with the total reaction cross section obtained from coupled-channels calculations for $^{58}Ni + ^{112,124}Sn$.

Target	$E_{c.m.}$ (MeV)	σ_{fus}[a] (mb)	σ_{di} (mb)	σ_{qe} (mb)	$\sum \sigma_i$[b] (mb)	σ_{cc} (mb)
^{112}Sn	191.1±1.0	280±40	165±35	205±30	650±80	785±100
	177.9±1.0	195±25	165±25	135±20	495±55	615±75
	163.5±1.0	50±10	50±10	55±10	155±20	245±30
	157.5±1.0	15±3	10±5	40±15	65±15	125±15
	151.2±1.0	2±0.5	4±2	25±10	31±10	50±10
^{124}Sn	197.6±1.0	465±65	230±55	540±80	1235±140	1345±95
	184.0±1.0	405±55	225±40	415±60	1045±110	1025±75
	169.0±1.0	190±30	140±25	250±40	580±65	615±45
	162.8±1.0	95±15	40±10	190±30	325±40	310±25
	156.4±1.0	20±4	10±6	115±20	145±25	150±15

[a]Sum of evaporation residues (Ref. 1) and fission yields.
[b]$\sum \sigma_i = \sigma_{fus} + \sigma_{di} + \sigma_{qe}$.

tions show that the nuclear part of inelastic excitation accounts for only a small fraction of the total quasielastic yields, it has not been included in the quasielastic cross sections.

A comparison between the total reaction cross section and the sum of the measured fusion, deep-inelastic, and quasielastic scattering yields as function of the incident center-of-mass energy is shown in Figs. 9 and 10 for $^{58}Ni + ^{112,124}Sn$ (see also Table II). The total reaction cross sections for $^{58}Ni + ^{124}Sn$ are, within the error bars, equal to the sum of the measured fusion, deep-inelastic, and quasielastic scattering yields. For $^{58}Ni + ^{112}Sn$ at energies below the Coulomb barrier a significant part of the total reaction cross sections is still unaccounted for. However, for this system no quasielastic scattering data are available below the Coulomb barrier and the quasielastic scattering yields at these energies were obtained from the measured cross sections above the barrier, using the shape of the measured quasielastic excitation function for $^{58}Ni + ^{124}Sn$ to extrapolate to the lower energies. This can induce large errors.

Figure 11 shows the strength of fusion, deep-inelastic, and quasielastic scattering relative to the total observed reaction cross sections for $^{58}Ni + ^{112,124}Sn$ as function of the incident center-of-mass energy. At energies above the Coulomb barrier the partition between the various reaction modes seems constant, with fusion and quasielastic scattering being the dominant modes for

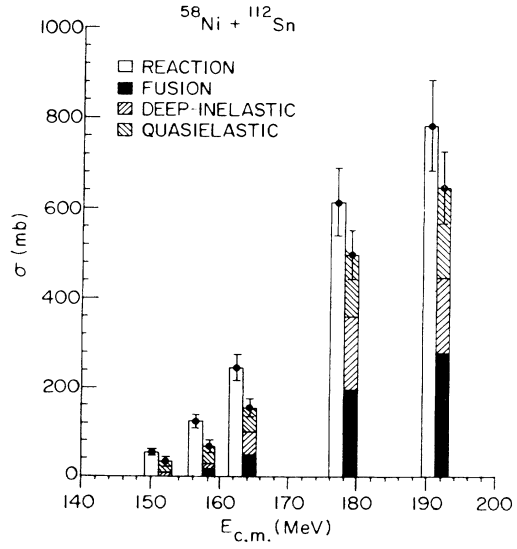

FIG. 9. Comparison between the total reaction cross sections obtained from coupled channel calculations, and the sum of measured fusion, deep-inelastic, and quasielastic scattering yields for $^{58}Ni + ^{112}Sn$.

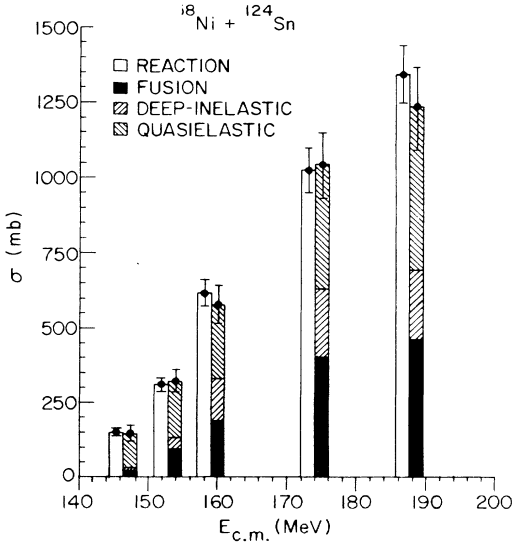

FIG. 10. Comparison between the total reaction cross sections obtained from coupled channel calculations, and the sum of measured fusion, deep-inelastic, and quasielastic scattering yields for $^{58}Ni + ^{124}Sn$.

^{58}Ni + ^{112}Sn and ^{58}Ni + ^{124}Sn, respectively. Below the barrier quasielastic scattering exhausts an increasingly larger fraction of the total reaction cross section for both systems studied. While fusion is stronger than deep-inelastic scattering at energies above the barrier, at sub-barrier energies the two are similar in yield.

C. Sub-barrier fusion enhancement

A large sub-barrier fusion enhancement is observed when the measured fusion cross sections are compared with results of one-dimensional barrier penetration calculation using the real part of the optical model potentials discussed in Sec. IV B (solid curves in Fig. 12). At energies above the barrier the calculated fusion cross sections are larger than the measured yields, indicating an inhibition of the formation of a compound nucleus, an effect which has been interpreted in terms of the extra-push model by Swiatecki.[22] This was discussed for the Ni + Sn system in Ref. 3.

In order to study the effect of coupling of channels to the entrance channel, I have carried out coupled-channels calculations, with the first 2^+ and 3^- states in both Ni and Sn, using the code PTOLEMY.[19] Fusion was defined by imposing an incoming wave boundary condition (IWBC) on the coupled wave equations[23] such that all flux within a radius of 10 fm was assumed to lead to fusion. The potential used in these calculations was the real part of the optical model potentials discussed in Sec. IV B. The results are shown by the dashed curves in Fig. 12. Although the coupling to the inelastic channels gives an increase of the calculated sub-barrier fusion yields, they are able to account for only a small part of the observed enhancement. This is not surprising since the nuclear inelastic cross sections are only a small fraction of the total quasielastic yields. It is entirely plausible that the coupling of the entrance channel to other quasielastic channels needs to be taken into account. Also the implications of the strength of deep-inelastic scattering on the sub-barrier fusion enhancement needs to be considered. Calculations including quasielastic transfer have been made so far only for light systems (^{16}O + ^{208}Pb, S + Ni).[23,24]

V. SUMMARY

Excitation functions of deep-inelastic scattering and fission have been measured for ^{58}Ni + ^{112,124}Sn at incident energies from 20 MeV below to 50 MeV above the Coulomb barrier. The calculated total reaction cross sections are in reasonable agreement with the sum of the fusion, deep-inelastic, and quasielastic scattering yields.

Deep-inelastic scattering is a strong reaction channel at all measured energies. The presence of deep-inelastic scattering at bombarding energies slightly above the barrier has been observed for other systems,[25–28] but this is the first detailed study of such a process at incident energies well below the Coulomb barrier. Although fusion is

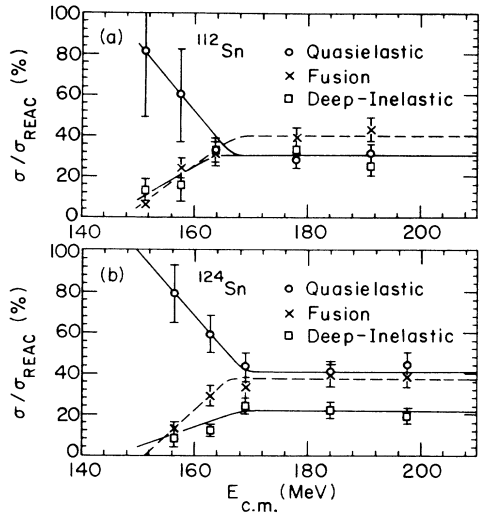

FIG. 11. Relative strength of quasielastic, deep-inelastic, and fusion scattering, relative to the sum of the individual yields for ^{58}Ni + ^{112,124}Sn as function of incident center-of-mass energy.

stronger than deep-inelastic scattering at energies above the barrier, it is similar in strength at energies below the barrier. The mass distributions of deep-inelastic scattering are peaked around masses close to those of projectile and target. The lower endpoint of the total kinetic energy spectra is independent of bombarding energy and consistent with large deformations in each reaction product ($\beta \simeq 0.65$). The angular distributions show two distinct components: one is peaked close to the grazing angle, the other shows an increase in yield towards forward

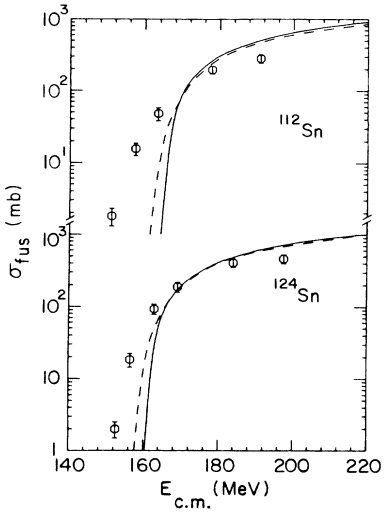

FIG. 12. Measured fusion cross sections for ^{58}Ni + ^{112,124}Sn compared with the results of IWBC calculations. The solid lines are for no coupling; results of including coupling to inelastic excited states in projectile and target are shown by the dashed curves.

scattering angles. At 270 and 290 MeV the measured strength of the forward peaked component is in reasonable agreement with predictions made using the one-body dissipation model, but the calculated yields for the backward peaked component are smaller than the measured cross sections. The existence of deep-inelastic scattering at energies below the Coulomb barrier indicates that the frictional force is still very effective even when the density overlap between projectile and target is rather small.

The sub-barrier fusion yields are much larger than the results of one-dimensional barrier penetration calculations. The coupling between elastic and inelastic channels gives a large increase of the calculated sub-barrier fusion yields, but they are able to account for only a small part of the observed enhancement, indicating the need to include coupling to other reaction modes, such as nucleon exchange.

ACKNOWLEDGMENTS

The author is grateful for many helpful and stimulating discussions with J. P. Schiffer, K. E. Rehm, and W. Henning during the course of this work and to D. Schull for supplying the ^{112}Sn target. The efforts of the ATLAS crew to provide reliable ^{58}Ni beams during this experiment was much appreciated. This work was performed at Argonne National Laboratory while a Laboratory-Graduate Participant. Program administered by the Argonne Division of Educational Programs with funding from the U.S. Department of Energy. This paper was presented as a thesis to the Department of Physics, The University of Chicago, in partial fulfillment of the requirements for the Ph.D. degree. This work was supported by the U.S. Department of Energy, Nuclear Physics Division, under Contract No. W-31-109-Eng-38.

[1]W. S. Freeman, H. Ernst, D. R. Geeseman, W. Henning, T. J. Humanic, W. Kühn, G. Rosner, J. P. Schiffer, B. Zeidman, and F. W. Prosser, Phys. Rev. Lett. **50**, 1563 (1983).

[2]K. T. Lesko, W. Henning, K. E. Rehm, G. Rosner, J. P. Schiffer, G. S. F. Stephans, B. Zeidman, and W. S. Freeman, Phys. Rev. Lett. **55**, 803 (1985).

[3]K. T. Lesko, W. Henning, K. E. Rehm, G. Rosner, J. P. Schiffer, G. S. F. Stephans, B. Zeidman, and W. S. Freeman, Phys. Rev. C **34**, 2155 (1986).

[4]W. Henning, F. L. H. Wolfs, J. P. Schiffer, and K. E. Rehm, Phys. Rev. Lett. **58**, 318 (1987).

[5]F. L. H. Wolfs, W. Henning, K. E. Rehm, and J. P. Schiffer, Phys. Lett. B (in press).

[6]G. Hempel, F. Hopkins, and G. Schatz, Nucl. Instrum. Methods **131**, 445 (1975).

[7]H. Stelzer, Nucl. Instrum. Methods **133**, 409 (1976).

[8]A. Breskin and N. Zwang, Nucl. Instrum. Methods **146**, 461 (1977).

[9]M. Just, D. Habs, V. Metag, and H. J. Specht, Nucl. Instrum. Methods **148**, 283 (1978).

[10]J. Galin, L. G. Moretto, R. Babinet, R. Schmitt, R. Jared, and S. G. Thompson, Nucl. Phys. **A255**, 472 (1975).

[11]L. G. Moretto, S. S. Kataria, R. C. Jared, R. Schmitt, and S. G. Thompson, Nucl. Phys. **A255**, 491 (1975).

[12]B. Tamain, F. Plasil, C. Ngô, J. Péter, M. Berlanger, and F. Hanappe, Phys. Rev. Lett. **36**, 18 (1976).

[13]L. G. Moretto, J. Galin, R. Babinet, Z. Fraenkel, R. Schmitt, R. Jared, and S. G. Thompson, Nucl. Phys. **A259**, 173 (1976).

[14]J. Péter, C. Ngô, F. Plasil, B. Tamain, M. Berlanger, and F. Hanappe, Nucl. Phys. **A279**, 110 (1977).

[15]V. E. Viola, Jr., Nuclear Data Sec. A **1**, 391 (1966).

[16]A. Gobbi, Nucl. Phys. **A354**, 337 (1981).

[17]H. Feldmeier, in *Nuclear Structure and Heavy Ion Dynamics*, edited by L. Moretto and R. A. Ricci (North-Holland, Amsterdam, 1984), p. 274.

[18]J. S. Blair, Phys. Rev. **95**, 1218 (1954).

[19]S. C. Pieper, M. H. Macfarlane, and R. Rhoades-Brown, Argonne Report ANL-76-11 (revised), 1976.

[20]A. M. van den Berg, W. Henning, L. L. Lee, K. T. Lesko, K. E. Rehm, J. P. Schiffer, G. S. F. Stephans, F. L. H. Wolfs, and W. S. Freeman, Phys. Rev. Lett. **56**, 572 (1986), and submitted to Phys. Rev. C.

[21]R. R. Betts, P. M. Evans, C. N. Pass, N. Poffé, A. E. Smith, L. Stuttgé, J. S. Lilley, D. W. Banes, K. A. Connel, J. Simpson, J. R. H. Smith, A. N. James, and B. R. Fulton, submitted to Phys. Rev. Lett.

[22]W. J. Swiatecki, Phys. Scr. **24**, 113 (1981); Nucl. Phys. **A376**, 275 (1982).

[23]S. C. Pieper, M. J. Rhoades-Brown, and S. Landowne, Phys. Lett. **162B**, 43 (1985).

[24]S. Landowne, Steven C. Pieper, and F. Videbaek, Phys. Rev. C **35**, 597 (1987).

[25]H. Essel, K. Hartel, W. Henning, P. Kienle, H. J. Körner, K. E. Rehm, P. Sperr, W. Wagner, and H. Spieler, Z. Phys. A **289**, 265 (1979).

[26]K. E. Rehm, H. Essel, P. Sperr, K. Hartel, P. Kienle, H. J. Körner, R. E. Segel, and W. Wagner, Nucl. Phys. **A366**, 477 (1981).

[27]A. C. Mignerey, K. L. Wolf, D. G. Raich, V. E. Viola Jr., J. R. Birkelund, W. U. Schröder, and J. R. Huizenga, Phys. Rev. C **29**, 158 (1984).

[28]W. Mayer, G. Beier, J. Friese, W. Henning, P. Kienle, H. J. Körner, W. A. Mayer, L. Müller, G. Rosner, and W. Wagner, Phys. Lett. **152B**, 162 (1985).